geometric deviation. The skewness of the distribution depends on the value of σ_g. At small values the skewness is reduced and the frequency curve approximates the normal distribution.

To obtain the fraction of particles between D_p and $D_p + dD_p$ the above probability density functions are integrated as indicated below:

$$P(D_{pi} < D_p < D_{pi} + dD_p) = F(D_{pi} + dD_p) - F(D_{pi}) \quad \text{(A3)}$$

$$= \int_{D_{pi}}^{D_{pi}+D_p} p(\xi)\, d\xi$$

where

$$F(D_p) = \int_{\infty}^{D_p} p(\xi)\, d\xi$$

and

$$\int_{-\infty}^{\infty} p(D_p)\, dD_p = 1$$

Some authors have modified the logarithmic density function by eliminating the diameter D_p in the denominator of Equation (A2).

$$p(D_p) = \frac{1}{(2\pi)^{1/2}\sigma_0} \exp\left[-\frac{(\log D_p - \log D_{pm})^2}{2\sigma_0^2}\right] \quad \text{(A4)}$$

Normalization of this equation leads to the zero-order logarithmic distribution function:

$$p(D_p) = \frac{\exp\left[-\dfrac{(\log D_p - \log D_{pm})^2}{2\sigma_0^2}\right]}{(2\pi)^{1/2}\sigma_0 D_{pm} \exp\left[\dfrac{\sigma_0^2}{2}\right]} \quad \text{(A5)}$$

This distribution is defined by two parameters: the modal diameter, D_{pm} and σ_0. D_{pm} can be expressed in terms of the mean diameter as shown below:

$$\ln \overline{D}_p = \ln D_{pm} + 1.5\,\sigma_0^2 \quad \text{(A6)}$$

and the standard deviation is related to σ_0 by the following equation:

$$\sigma = D_{pm}[\exp(4\sigma_0^2) - \exp(3\sigma_0^2)]^{1/2} \quad \text{(A7)}$$

Espenscheid et al. (1964) and Kerker (1969) describe some of the properties of the zero-order logarithmic distribution, which is used in analyzing the light scattering measurements by either the polarization ratio of specific intensity methods.

Manuscript received July 10, 1972; revision received January 26, 1973, and accepted January 29, 1973.

Enhancement of Stagnation Flow Heat and Mass Transfer Through Interactions of Free Stream Turbulence

At the forward stagnation point of a bluff body the laminar flow is influenced by externally generated free-stream turbulence, such as from grids, in such a way that heat and mass transport are significantly enhanced above their normal values. The basis of this enhancement is an unsteady, three-dimensional flow pattern formed at the forward stagnation point and triggered or altered by the free-stream turbulence. Such complex flows can be interpreted as roll cells oriented with their axes parallel to streamwise coordinates. Such roll cells have been observed by other investigators using special experimental visualization techniques. This complex flow was introduced into the momentum and transport equations, which were then solved numerically to produce the relationships between Nusselt, Reynolds, and Prandtl numbers and free-stream turbulence. Not only were these relationships nearly identical with earlier established empirical correlations, but they revealed in addition a strong augmentation for high Prandtl number flows. Predictions in slurry flows around bluff bodies were also found to be reasonable.

T. R. GALLOWAY

University of California
Berkeley, California

SCOPE

One of the most commonly encountered problems in the chemical and petroleum process industries is that of heat or mass transfer from a cylindrical or spherical surface to the fluid flowing past it. The cylinders can be heat exchanger tubes, column packing, catalyst pellets, etc., and spheres can be droplets, bubbles, bed or catalyst packing, etc. The fluid can be gas or liquid and can contain particulates of solid or other phases. In nearly all these cases the

T. R. Galloway is Assistant Director of the Sanitary Engineering Research Laboratory, Richmond Field Station, Richmond, California 94804.

fluid is in turbulent motion before it encounters the bluff body. In contrast to aerospace problems, many cases involve liquids where the Prandtl or Schmidt numbers are much greater than unity. Therefore, it is relevant to ask what is known about the flow of a high Prandtl number turbulent fluid past a bluff body (see Figure 1).

The laminar boundary layer formed in the region of the forward stagnation on a bluff body, such as a cylinder or sphere, responds to artificially generated free-stream turbulence in such a way that heat and mass transfer rates are significantly increased. The fact that a flow thought to be laminar could be affected by external eddies has been a point of considerable controversy. Theoretical and experimental work (by Sadeh et al., 1970) has recently revealed the true three-dimensional character of this laminar flow and showed formation of roll cells oriented lengthwise along the streamwise axis. A mechanism of vorticity amplification (Sadeh et al., 1970) in the stagnation flow appears to explain the phenomenon of roll cell formation and its linkage to free-stream turbulence.

The controversial effect of free-stream turbulence on stagnation flow transport was experimentally demonstrated by specially designed studies on cylinders and spheres by Galloway and Sage (1967, 1972). In addition, extensive multiple regression analysis of the available literature was done to demonstrate the experimental limitations and extent of this enhancement phenomena. Figure 2 is a summary.

During the decade of experimental studies involving free stream turbulence there have been a number of advances by several research groups toward understanding the mechanism responsible for this observed enhancement, and it seems that it is time to attempt to unify some of this work. The series of publications of J. Kestin and co-workers and others is especially noteworthy, beginning with the identification of the importance of streamwise acceleration on augmented heat transfer from a flat plate (Kestin et al., 1961; Buyuktur et al., 1964; Junkhan et al., 1967) and the role of vorticity at a stagnation point (Sutera et al., 1963; Sutera, 1965) and leading up to the recent Kestin and Wood (1970) stagnation flow instability mechanism. Kuethe and co-workers (1961) and Smith and Kuethe (1966) have also examined the turbulence field produced at a stagnation point with similar conclusions. The flow visualization experiments of Kline and Reynolds and coworkers (Runstadler et al., 1965) have revolutionized our thinking about turbulent boundary layers. The notion of relaminarization or turbulization through streamwise pressure gradients or sharp temperature profiles normal to the surface has helped to apply these ideas. It has even been possible to quantify such manipulations (Kearney et al., 1970).

Also in the last five years there have been many considerable advances in machine computation of turbulent boundary layers, the Stanford Olympics on turbulence (Stanford, 1968) offering an excellent comparison of computing methods. However, none of these methods available today treat the problem of free stream turbulence interacting with a laminar boundary layer as exists at a forward stagnation point of a bluff body and as it develops along the streamwise direction. It is the purpose of this paper to unify many of these ideas of roll cell formation, bluff body stagnation flow, effects of free stream turbulence on laminar boundary layers, and machine computation of turbulent boundary layer equations.

Here a new twist is used to conventional approaches which use idealized eddy coefficient models. This involves beginning with a real free-stream turbulence-sensitive, three-dimensional roll cell flow, and deriving a two-dimensional eddy law which is used in solving the momentum and transport equations in order to predict the experimentally observed enhancement of stagnation transport with free-stream turbulence. This path from the roll cell to transport enhancement ties together many of the loose ends in the literature.

In addition, an extension to high Prandtl number has been possible using the law of the wall eddy model approach like that of Smith and Kuethe (1966). The increased magnitude of this enhancement process for high Prandtl number fluids has been predicted by Galloway and Sage (1964) using the simplest turbulent integral approaches.

Two cases are considered for deriving relationships between the instantaneous flow field and its alteration by free stream turbulence: 1. The law of the wall; and 2. Roll cell flow. The basic laminar fluid mechanics are handled by extending the nonsimilar asymptotic expansion of Merk (1959). The idea of using an eddy coefficient is merely one of convenience: of lumping the complexities of unsteady, three-dimensional flows into a single term which can be handled in an extended Merk expansion. This is not to be confused with techniques for solving well-developed turbulent flow problems.

CONCLUSIONS AND SIGNIFICANCE

Numerical solutions by Merk similarity analysis to the equations of motion and transport with both a law of the wall and roll cell stagnation flow model yield a result which has almost identical form to the correlation established earlier by the author using stochastic and empirical arguments. This correlation which is widely used in chemical engineering design now has a theoretical basis. The most significant theoretical result is that the transport augmentation depends upon the term $IRe^{1/2}\ \sigma^{1/6}/\sigma_t$. The Prandtl or Schmidt numbers σ have a significant effect on augmentation. The geometry of the bluff body has little effect since the enhancement is only 11.41% larger for spheres than cylinders. The parameter χ has physical interpretation as response within the sublayer resulting from external perturbations, such as free stream turbulence, particles, etc. It does involve terms from the pressure gradient, and it is clear that the negative pressure gradient is a necessary condition for augmentation effects.

Comparisons with the flat plate universal turbulent velocity profile $u^+ = y^+$, in the sublayer indicate that the phenomenon responsible for augmentation is located near the wall, well within the sublayer. This region is also the region where flat plate three-dimensional streamwise roll cells have been observed. A roll cell model was formulated and simplified into the form of an eddy coefficient and the transport equations were solved to obtain the stagnation point transport enhancement from free-stream turbulence. Available experimental data for the enhancement allow one to obtain the required roll cell circulation strength which at high turbulence levels can be expressed as $A = 0.193\ U_\infty I/D$. The magnitudes are typically in the 0.1 to 100 Hertz range which is in agreement with hot wire observations. The roll cell mechanism appears to be a reasonable one for explaining this enhancement process.

AUGMENTATION OF LAMINAR STAGNATION TRANSPORT FROM FREE-STREAM TURBULENCE

The development begins with equations of continuity, momentum, heat, and molecular species (Schlicting, 1960; Bird et al., 1960) by applying the Merk similarity transformations for the stream functions:

$$\Psi = U_\infty L\left[\frac{2\xi}{Re}\right]^{1/2} F(\xi,\eta) \tag{1}$$

where

$$\xi = \int_0^x \frac{U_1(x)}{U_\infty}\left(\frac{r(x)}{d}\right)^{2k} d\left(\frac{x}{d}\right)$$

$$\eta = \left[\frac{Re}{2\xi}\right]^{1/2} \frac{U_1(x)}{U_\infty}\left(\frac{r(x)}{d}\right)^{k}\left(\frac{y}{d}\right)$$

$$Re = \frac{U_\infty d}{\nu}$$

For two-dimensional flow, $k = 0$, and for axisymmetric flow, $k = 1$.

Law of the Wall Flow

Since our attention is directed to heat and mass transfer, an eddy law is desired which is especially applicable to the wall region. The simplest concept is that of Prandtl's mixing length. Here we use the Schlicting (1960) definitions of the eddy coefficients and from Prandtl note:

$$|u'| \propto |v'| = l\frac{\partial U}{\partial y} \tag{2}$$

where Prandtl's mixing length $l = k'y$. If we note

$$\overline{u'v'} \propto \overline{|u'|}\,\overline{|v'|} = |u'|\,k'y\frac{\partial U}{\partial y} = \epsilon_m\frac{\partial U}{\partial y} \tag{3}$$

Then the eddy law becomes

$$\epsilon_m = kIU_\infty y \tag{4}$$

as first identified by Smith and Kuethe (1966) where the intensity of turbulence in the free stream is defined at a reference position in the flow field corresponding to the bluff body forward stagnation with the body removed. I is taken to be the external driving force which sets the level of the fluctuating velocity $|u'|$ near $x, y = 0$

$$|u'| \propto U\,I$$

The similarity variable describing this eddy law becomes

$$\chi = kI\left(\frac{U_\infty}{U_1}\right)^k [2\xi Re]^{1/2} \tag{5}$$

Also the similarity variable involving the streamwise pressure gradient becomes

$$\beta = 2\xi\left(\frac{U_\infty}{U_1}\right)\left(\frac{d}{r}\right)^{2k}\frac{d(U_1/U_\infty)}{d(x/L)} \tag{6}$$

With these transformations the equation of motion reduces to the following:

$$(1+\chi\eta)F_{\eta\eta\eta} + (F+\chi)F_{\eta\eta} + \beta(1-F_\eta^2) = 2\xi(F_\eta F_{\xi\eta} - F_\xi F_{\eta\eta}) \tag{7}$$

where the subscripts denote partial differentiation with respect to that variable. The left-hand side reduces to the Falkner-Skan Equation when $\chi = 0$.

Roll Cell Flow

A roll cell flow can also be used to derive an eddy law. If one postulates a Gortler (1954, 1957) type instability arising from the sharply curved streamlines in the vicinity of the forward stagnation point or a vorticity stretching and amplification mechanism (Sutera, 1963), roll cells can be formed with their axes parallel to the streamlines, their strength of rotation A dependent upon streamline curvature, free stream velocity and turbulence, and their wave number α dependent upon Reynold's number and free stream turbulence. The vector velocities W_r, V_r can be written down by intuition much as done by Ruckenstein and Berbente (1970) with spanwise periodicity in Z:

$$W_r = 2\,Ay\ \mathrm{SIN}\ (\pi Z/\lambda) \tag{8}$$

$$V_r = \frac{\pi Ay}{\lambda}\ \mathrm{COS}\ (\pi Z/\lambda) \tag{9}$$

Since the turbulent vorticity near the surface is now represented by roll cells, the fluctuating velocities u' and v' appearing in the definition of the eddy viscosity:

$$\epsilon_m = \frac{\overline{(W')\,(V')}}{(-\partial W/\partial y)} = \frac{\pi Ay^3}{\lambda}\frac{\int_0^{\lambda/2}\mathrm{SIN}\frac{\pi Z}{\lambda}\mathrm{COS}\frac{\pi Z}{\lambda}\,d\left(\frac{\pi Z}{\lambda}\right)}{\int_0^{\lambda/2}\mathrm{SIN}\frac{\pi Z}{\lambda}\,d\left(\frac{\pi Z}{\lambda}\right)} \tag{10}$$

are replaced by W_r and V_r from Equations (8) and (9). The eddy viscosity becomes

$$\epsilon_m = \frac{\pi A}{2\lambda}y^3 \tag{11}$$

when appropriately averaged over one complete roll cell. It has been shown by Sutera et al., (1963, 1965) that a turbulent free-stream can carry vorticity into the boundary layer at a stagnation point, upsetting its stability and leading to three-dimensional roll cells in the laminar flow. When the wave length is above a critical neutral wave length $\lambda_0 = \pi d\ Re^{-1/2}$, vorticity amplification can occur. Kestin and Wood (1970) present experimental evidence as well as an instability analysis for the effect of free-stream turbulence on the intensity of roll cell circulation and their spacing. They show the spacing to decrease 25% as free stream turbulence level varies from 0 to infinity, at constant Reynold's number, and suggest that the amplification factor, and therefore the rotational strength A, (sec^{-1}), increase with increasing free-stream turbulence. In this paper we will establish quantitatively how the dimensionless circulation strength group AD/U_∞ increases with increasing free-stream turbulence as reflected by augmented stagnation point heat transfer.

Other more general roll cell models with higher Y dependence than in Equations (8) and (9) can be formulated producing eddy coefficients as in Equation (11) but depending on y^n. Accordingly, the similarity variable χ_n becomes

$$\chi_n = \frac{\pi A\lambda}{2(n-2)U_\infty}\left(\frac{d}{\lambda}\right)^{n-1}\left(\frac{U_\infty\sqrt{2\xi}}{U_1}\right)^n \tag{12}$$

valid for $n \geqq 3$. The new transformed equation of motion becomes

$$(1+\chi_\eta\,\eta^n)F_{\eta\eta\eta} + (F + n\chi_n\,\eta^{n-1})F_{\eta\eta} + \beta(1-F_\eta^2) = 2\xi\,[F_\eta F_{\xi\eta} - F_\xi F_{\eta\eta}] \tag{13}$$

and similarly for the transport of heat or molecular species

$$\left[\frac{1}{\sigma}+\frac{\chi_\eta\,\eta^n}{\sigma_t}\right]\theta_{\eta\eta}+\left[F+\frac{n\chi_n\,\eta^{n-1}}{\sigma_t}\right]\theta_\eta = 2\xi\,[\theta_\xi F_\eta - F_\xi\theta_\eta] \tag{14}$$

where for heat transfer $\sigma = Pr$ and mass transfer $\sigma = Sc$, and where σ_t denotes either the turbulent Prandtl number, $Pr_t = \epsilon_m/\epsilon_h$ or turbulent Schmidt number, $Sc_t = \epsilon_m/\epsilon_d$.

The last term in Equation (12) greatly complicated the series development since χ_η and β expansions in terms of (X/D) must be combined with the right-hand sides of Equations (13) and (14) and grouped into like powers of (X/D). For solutions near stagnation, however, the last term of Equation (12) is just a constant $u_1{}^{-n/2}$, where u_1 is the first coefficient of the outer flow velocity expansion, $U_1(X)$.

Using these functions F and θ and their derivatives, the general form of the skin friction coefficient valid for a wide range of flow geometries and outer velocity profiles $U_1(X)$, can be written down as

$$C_f = 2\frac{U_1}{U_\infty}\frac{1}{Re^{1/2}}\left[\frac{d(U_1/U_\infty)}{\beta d(X/d)}\right]^{1/2} F_{\eta\eta}\,(\xi,0) \tag{15}$$

As well as the general Frossling group

$$Fs = \frac{-\theta_n(0)}{\sigma^{1/3}}\left[\frac{d(U_1/U_\infty)}{\beta d(X/d)}\right]^{1/2} \tag{16}$$

METHODS OF SOLUTION

A number of methods of solution to Equations (13) and (14) were tried and a few will be briefly summarized so that others might learn from this experience. At first, a full series solution for two-dimensional flow was attempted, expanding

$$F(\xi,\eta) = \sum_{i=0}^{\infty}\xi^{1/2}\sum_{j=2}^{\infty}A(j,i)\,\eta^j \tag{17}$$

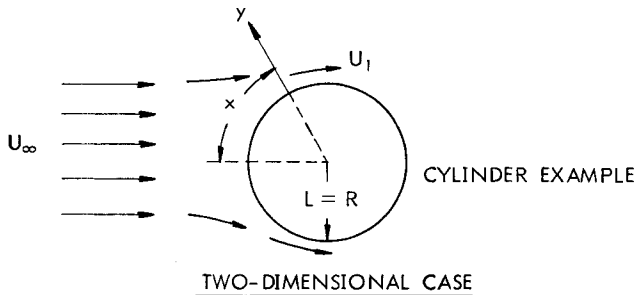

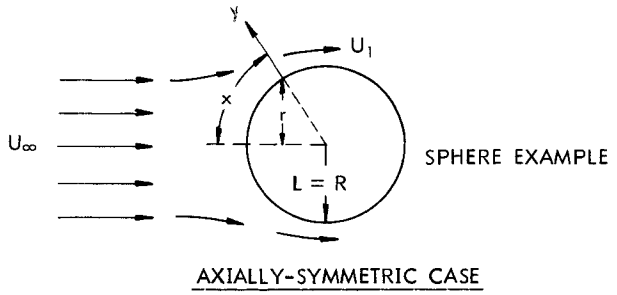

Fig. 1. System of coordinates.

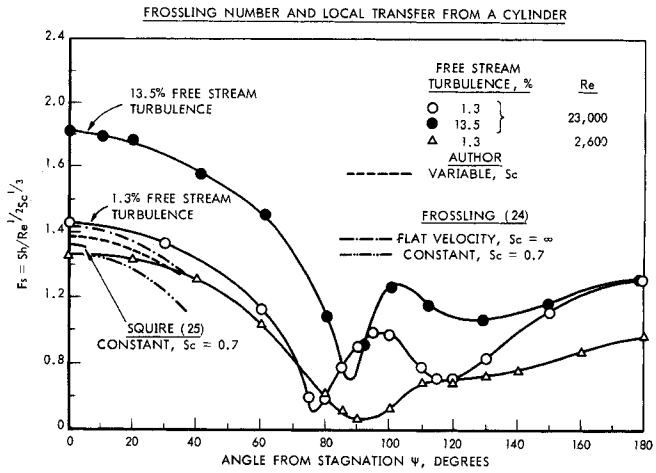

Fig. 2. Frossling number and local transfer from a cylinder.

and

$$U_1(X) = \sum_{i=1}^{\infty}u_iX^i$$

Recursion formulae for the Prandtl mixing length model were typically as follows:

$$A(3,0) = -1/6\,[2\,A(2,0)\chi(0)+\beta_0]$$
$$A(4,0) = \frac{\chi(0)}{-12}\,[2\,A(2,0)\chi(0)+\beta_0] \tag{18}$$
$$\ldots \text{ etc.}$$

Requiring compatible coefficients for the expansion of

$$\beta(\xi) = \sum_{i=0}^{\infty}\beta_i\,\xi^{i/2}$$

$$\beta_0 = 1,\quad \beta_1 = \frac{2}{u_1}\left[\frac{2}{3}\frac{u_2}{u_3}\right]$$
$$\beta_2 = \frac{2}{u_1{}^3}\left[\frac{3}{2}u_1u_3-\frac{11}{9}u_2{}^2\right] \tag{19}$$
$$\beta_3 = \left(\frac{2}{u_1}\right)^{3/2}\cdot\frac{1}{u_1{}^3}\left[\frac{12}{5}u_1{}^2u_4 - \frac{27}{6}u_1u_2u_3+\frac{59}{27}u_2{}^3\right]$$
$$\ldots \text{ etc.}$$

and for $\chi(\xi) = \sum_{i=0}^{\infty}\chi_i\xi^{i/2}$

$$\chi_0 = -kIU_\infty Re^{1/2},\quad \chi_1 = \left(\frac{2}{u_1}\right)^{1/2}\left[\frac{2u_2}{3u_1}\right]\chi_0$$
$$\chi_2 = \frac{2}{u_1{}^3}\left[\frac{3}{4}u_1u_3-\frac{5}{6}u_1{}^2\right]\chi_0 \tag{20}$$
$$\ldots \text{ etc.}$$

A similar series expansion was used for $\theta(\xi,\eta)$

$$\theta(\xi,\eta) = \sum_{i=0}^{\infty}\xi^{i/2}\sum_{j=0}^{\infty}b(j,i)\,\eta^j \tag{21}$$

Some examples of the results are given for circular cylinders in laminar potential flow and these compare well with those by Squire (1942) done for $\sigma = 1$:

$$Fs = \frac{Nu \text{ or } Sh}{Re^{1/2}\,\sigma^{1/3}} = 1.324\,(1 - A_2\xi^2 - A_4\xi^4 - \ldots)\,[1 + \phi_1(\sigma)]^{-1} \quad (22)$$

where

$$\phi_1(\sigma) = \frac{0.114}{\sigma^{1/3}} - \frac{0.0146}{\sigma^{2/3}} - \frac{0.106}{\sigma} + \frac{0.0170}{\sigma^{4/3}} + \frac{0.0048}{\sigma^{5/3}}$$

A similar analysis for axisymmetric flow yields the following result for spheres:

$$Fs = \frac{(Nu \text{ or } Sh) - 2}{Re^{1/2}\,\sigma^{1/3}} = 1.471\,(1 - A_2{}^1\xi^2 - A_4{}^1\xi^4)\,\frac{1}{1 + \phi_2(\sigma)} \quad (23)$$

$$\phi_2(\sigma) = \frac{0.0840}{\sigma^{1/3}} - \frac{0.00790}{\sigma^{2/3}} + \frac{0.001325}{\sigma} - \frac{0.00406}{\sigma^{4/3}} + \frac{0.00317}{\sigma^{5/3}}$$

These low turbulence, series solutions have been most useful in revealing the analytical form of the Frossling group (Fs), and its residual dependence on Pr or Sc; however, they also reveal the critical importance of accurately satisfying the velocity boundary condition at infinity. Asymptotic matching of inner and outer solutions proved helpful but required a priori knowledge of the functional dependence.

Accounting for effects of free stream turbulence or suspended particulates at large enough levels for practical design work in the process industries was quite difficult by series solution since the coefficients as in Equation (16) become large in number and very complex algebraic functions of dP/dx and the eddy coefficients. The larger the eddy coefficients become the more the number of terms in the series are required in order to apply the velocity boundary condition at infinity. FORMAC, IBM's algebraic manipulating language, both the FORTRAN and PL/I version, was used to generate the required number of terms in the expressions. Both proved to be expensive in execution time ($10 per term) and most difficult to debug and check. The FORTRAN version was designed to run on the IBM 7090 and the PL/I version on IBM 360/50. The FORTRAN version eventually produced correct results, whereas in the PL/I version a number of system errors were turned up which have remained unsolved by IBM.

The high cost of full series solution to the problem led to the adoption of hybrid series and numerical solution. This scheme involved solving the equation of motion Equation (13) and the transport equations Equation (14) numerically instead of by series and then carrying out a nonsimilarity series in distance from stagnation by FORMAC assisted algebraic techniques as before. To date the nonsimilarity series has been completed together with the numerical solution at the forward stagnation point. It is the latter solution which constitutes the main contribution of this paper. The series expansion techniques and limited results are completed for the streamwise variation in ξ and will be presented in a subsequent paper. Here we shall concentrate on the numerical results in the vicinity of the forward stagnation point.

The numerical technique used to solve the left-hand sides of Equations (13) and (14) was the Gill modification of a fourth-order Runge-Kutta procedure in double precision arithmetic to solve N simultaneous first-order, variable coefficient, ordinary differential equations, with $N \leq 50$. Here by substitution Equations (13) and (14) involve five ordinary differential equations. The calculation was carried out on the Univac 1108. Fifty steps in η for a laminar case took one second of CPU time ($2.33) and the average turbulent run with 3,000 steps cost $16. The computation time increased very considerably for highly turbulent cases since the velocity boundary condition at infinity had to be applied at large values of η, sometimes as high as 35, and smaller steps as low as $\Delta\eta = 0.003$ were needed to keep the cumulative error always well under 0.1% in $F_\eta(0) = 1$.

NUMERICAL RESULTS

The results for the velocity profile for the two-dimensional case of a circular cylinder are shown in Figure 3, for various levels of free stream turbulence and Reynolds number corresponding to χ from 0 to 4.0. For the completely laminar case a detailed comparison is made in Table 1 between the universal velocity profiles obtained by each contributor. In the present work the highest laminar accuracy was needed in order to carry out the turbulent profile computations within 0.1%. In all cases agreement is to the last decimal place. It is believed that

TABLE 1. LAMINAR UNIVERSAL VELOCITY PROFILE, $F_\eta(0)$, FOR CIRCULAR CYLINDER

η	Tifford (1954) and Schlichting (1960)	Gortler (1957)	Bickley (Rosenhead, 1963)	Present work
0.00	0.2266	0.0000 00	0.0000 000	0.0000 0000 000
0.60	0.5663	0.5662 80	0.5662 805	0.5662 8050 965
1.20	0.8467	0.8466 71	0.8466 711	0.8466 7110 314
1.80	0.9568	0.9568 33	0.9568 338	0.9568 3378 446
2.40	0.9905	0.9905 49	0.9905 494	0.9905 4939 430
3.00	0.9984	0.9984 24	0.9984 242	0.9984 2415 492
3.60	0.9998	0.9998 03	0.9998 032	0.9998 0324 616
4.20	1.0000	0.9999 81	0.9999 819	0.9999 8185 032
4.80	1.0000	0.9999 98	0.9999 988	0.9999 9877 591
5.40	1.0000	0.9999 99	0.9999 999	0.9999 9990 388
6.00	1.0000	1.0000 00	1.0000 000	0.9999 9999 789
6.60	1.0000	1.0000 00	1.0000 000	0.9999 9999 994
7.20	1.0000	1.0000 00	1.0000 000	1.0000 0000 000
7.80	1.0000	1.0000 00	1.0000 000	1.0000 0000 000
			$F_{\eta\eta}(0)$	
0.00	1.2326	1.2325 87	1.2325 88	1.2325 8765 14

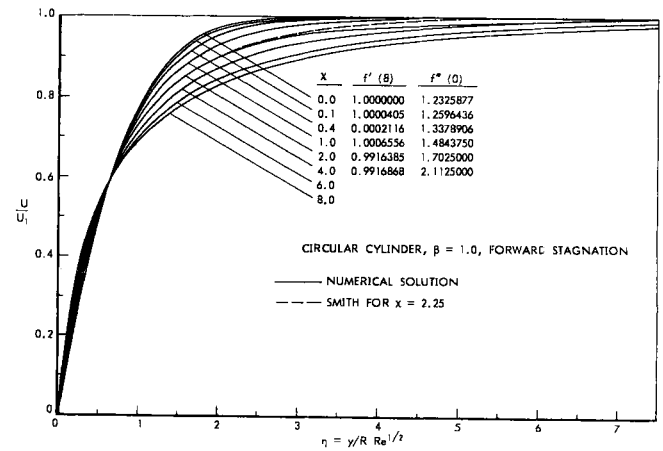

Fig. 3. Two-dimensional flow velocity profile.

differences at high turbulence level between Smith and Kuethe (1966) $\chi = 2.25$ and the present work arise from the former's accumulated error in the numerical method associated with satisfying the velocity boundary condition at infinity. A similar comparison has been made in Table 2 for spheres. Both comparisons for cylinders and spheres illustrate that high enough accuracy is possible with the current method in order to carry out reliable computations at high turbulence.

The first test of the computation gives the effects of free-stream turbulence expressed as $IRe^{1/2}$ on the shear rate at the forward stagnation point of a circular cylinder in cross flow as shown in Figure 4. Two calculations were done for coefficients of proportionality between χ and $IRe^{1/2}$ of 0.1000 and 0.082, the latter corresponding to Smith's $(k/2)$. The differences between Smith's and the present results arise from the uncertainties in the former's technique of satisfying the boundary condition $f'(6) = 1$. This work shows that errors below 0.1% are possible only if $f'(30) = 1$. Another computation involving shear rate for the coefficient of proportionality of 0.1 also is in good agreement with the experimental data; therefore, it should be concluded that the shear rate measurements suggest coefficients lying somewhere between 0.1 and 0.082.

It is most interesting to note that this theory with an eddy model consisting of the law of the wall predicts the

TABLE 2. LAMINAR UNIVERSAL VELOCITY PROFILE, $F_\eta(0)$, FOR SPHERE

η	Frossling (1958)	Rosenhead (1963)	Present work		
0.00	0.0000	0.0000	0.0000	0000	000
0.60	0.4669	0.4669	0.4668	9083	018
1.20	0.7614	0.7614	0.7614	6224	928
1.80	0.9142	0.9142	0.9142	0357	701
2.40	0.9760	0.9761	0.9760	6876	083
3.00	0.9949	0.9950	0.9949	5945	386
3.60	0.9992	0.9992	0.9992	1323	940
4.20	0.9999	0.9999	0.9999	1020	134
4.80	1.0000	1.0000	0.9999	9257	754
5.40	1.0000	1.0000	0.9999	9955	889
6.00	1.0000	1.0000	0.9999	9958	125
6.60	1.0000	1.0000	0.9999	9999	943
7.20	1.0000	1.0000	0.9999	9999	999
7.80	1.0000	1.0000	1.0000	0000	000
		$F_{\eta\eta}(0)$			
0.00	0.9277	0.9278	0.9276	8004	000

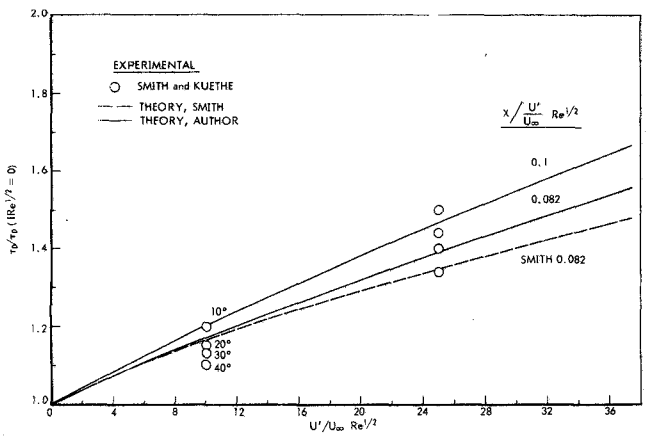

Fig. 4. Augmentation of surface shear rate on the forward stagnation of a cylinder.

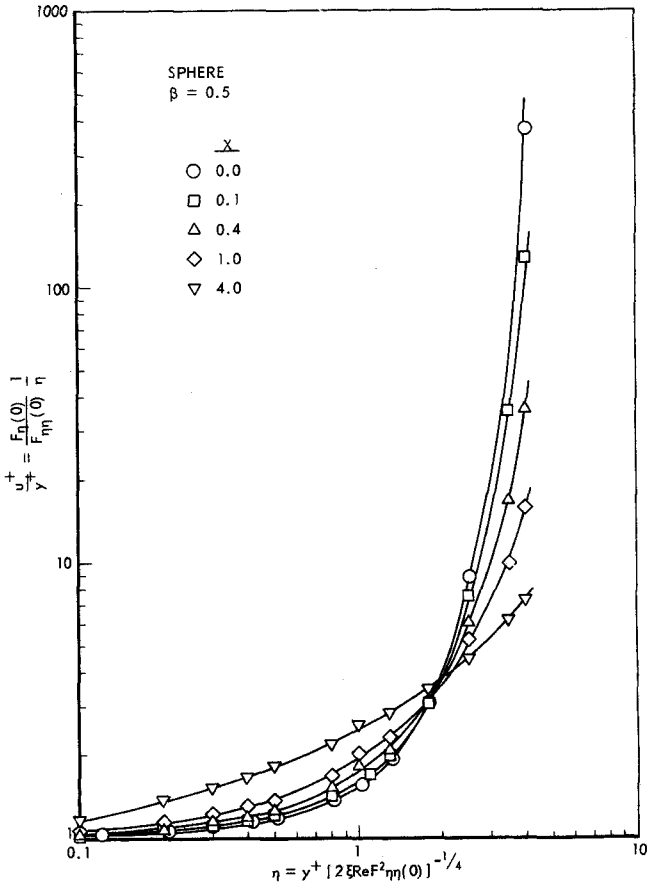

Fig. 5. Universal turbulent velocity profile, u^+ versus y^+.

flat plate classical universal turbulent velocity $u^+ = y^+$ in the laminar sublayer as shown in Figure 5 for spheres. The distance parameter $y^+ = 5$ is around $\eta = 0.4$. Note that as the turbulence level in the free stream is increased, an earlier transition occurs to the higher value of u^+ expected in the buffer layer. This can also be interpreted as a shrinking of the sublayer and inward expansion of the buffer layer. The results indicate that the important phenomena responsible for heat and mass transfer augmentation from a surface are occurring in the laminar sublayer where three-dimensional (stream-wise axis) roll cells are formed (Runstadler et al., 1965).

The effects of turbulence on the temperature or concentration profile have been shown in Figure 6 for χ varying from 0.0 to 0.8 and $\sigma = \sigma_t = 1$. It is most obvious from these profiles the importance of applying $f'(\infty) = 1$ at η considerably above 6. It is most interesting to note from these results that all profiles pass through $\theta = 0.455$ at $\eta = 1$ and that below $\eta = 1$ there are significant effects of turbulence. These latter effects explain why from Equation (16) the Frossling number ($Nu/Re^{1/2}Pr^{1/3}$ or $Sh/Re^{1/2}Sc^{1/3}$), which is for potential flow just $2\theta'(0)/\sigma^{1/3}$ for cylinders and $6^{1/2}\theta'(0)/\sigma^{1/3}$ for spheres for $\sigma > 1$, depends so strongly on $IRe^{1/2}$ as indicated by earlier experimental results. (Kestin, 1961; Galloway & Sage, 1964, 1967, 1972). This augmentation is also tabulated in Figure 6. A comparison of these results, $Fs = 1.14094$ for $\chi = 0$ and $\sigma = \sigma_t = 1$, with those of Evans (1968) indicates results identical to six significant figures.

The effects of turbulent Prandtl or Schmidt numbers σ_t appear to be simply that of scaling χ by σ_t. However, the function F in Equation (14) also depends on χ so that the actual relationship between θ and χ/σ_t can only

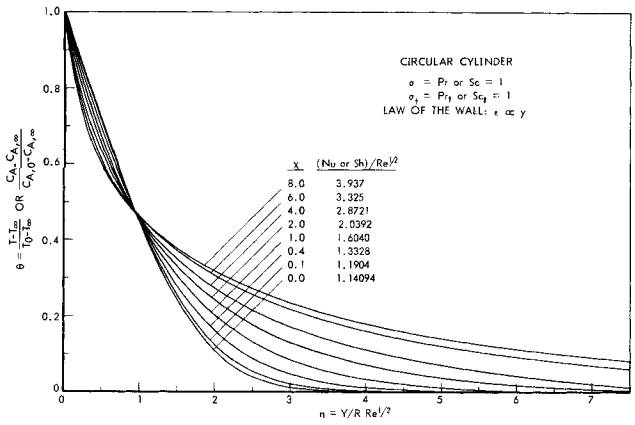

Fig. 6. Profiles normal to the surface.

be obtained by computation as in Figure 4. The profiles in Figures 6 and 7 are so nearly identical when χ is scaled by σ_t (for example, χ/σ_t) that one must conclude that any differences could well arise from cumulative errors in the numerical method alone. Hereafter, in studying effects of σ on θ the variable χ/σ_t will be used to reduce the number of variables to be explored numerically.

For the point of gaining physical insight, Figure 8 has been prepared to illustrate the large effect that σ has on the θ profile and also on the transport boundary layer thickness. It is significantly larger than the effects of turbulence shown in Figures 6 and 7. In fact, one would expect that the effects of turbulence would be felt more seriously on the thin transport boundary layer ($\sigma > 1$) where $\theta'(0)$ or Fs are very sensitive functions of the profile near the wall. This is illustrated in Figure 9. The Frossling number Fs depends weakly upon σ for $\sigma < 1$; that is, $Fs \alpha \sigma^{1/6}$. It is invariant with σ for $\sigma >> 1$ as $Fs = 1.3215$ for cylinders and $Fs = 1.4723$ for spheres. An asymptotic function which fits this behavior well at the forward stagnation point is as follows:

Cylinders:

$$Fs = \frac{1.3215}{[1 + 0.5768\,\sigma^{-1/2}]^{1/3}} \qquad 10^{-4} < \sigma < 10^{7} \qquad (24)$$

Spheres:

$$Fs = \frac{1.4723}{[1 + 0.4357\,\sigma^{-1/2}]^{1/3}} \qquad 10^{-4} < \sigma < 10^{7} \qquad (25)$$

Also shown for comparison in Figure 9, as a dashed curve, is the approximate series solution discussed earlier. It agrees well with the numerical work but deviates slightly at lower σ owing to the approximate nature of the series inversion and other series manipulating techniques.

The increasing augmentation with turbulence as σ increases is obvious in Figure 9 for both the law of the wall and the roll cell model (with $n = 3$). At $\sigma = 10$ the Frossling number is augmented 20% for the law of the wall model as the turbulence parameter χ increases from 0.0 to 0.1, whereas at $\sigma = 1.0$ the augmentation is only 5% for the law of the wall and 30% for the roll cell model. For various σ the augmentation is almost linear with χ/σ_t as illustrated for both models in Figure 10, with a slight downward curvature. This near linear relationship, $Fs \alpha Re^{1/2}$ with the coefficient of proportionality involving the free stream turbulence level I was established earlier using stochastic arguments and a quasi-integral approach and was subsequently verified experimentally (Galloway and Sage, 1964, 1967, 1972). Furthermore, it was also argued (Galloway, 1964) that the proportionality would depend weakly on σ and σ_t. Later least square functional analysis (Galloway and Sage, 1967) of extensive literature experimental data revealed a weak dependence on σ as $\sigma^{1/6}$. This σ dependence shown in Figure 10, surprisingly, is well represented by

$$Fs = A + B\left(\frac{\chi}{\sigma_t}\right)\sigma^{1/6} \qquad (26)$$

where A is given by Equation (24) and B is taken em-

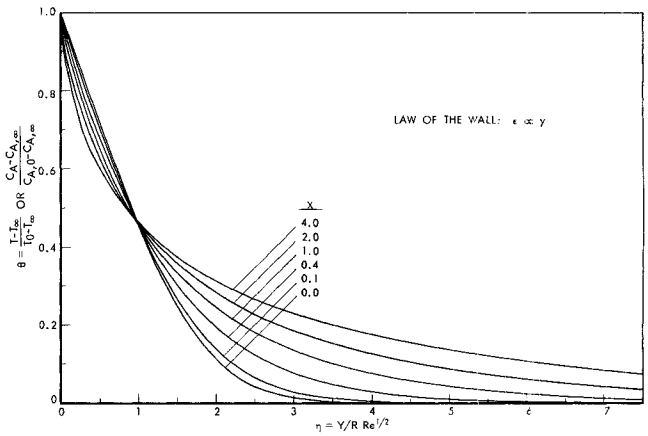

Fig. 7. Cylinder Θ profiles for $\sigma_t = 0.5$.

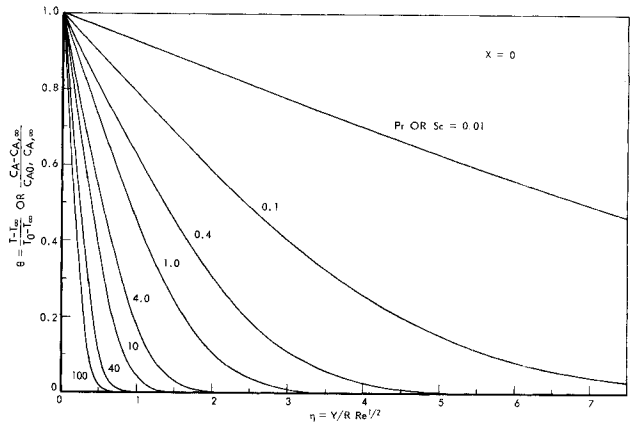

Fig. 8. Two-dimensional stagnation point.

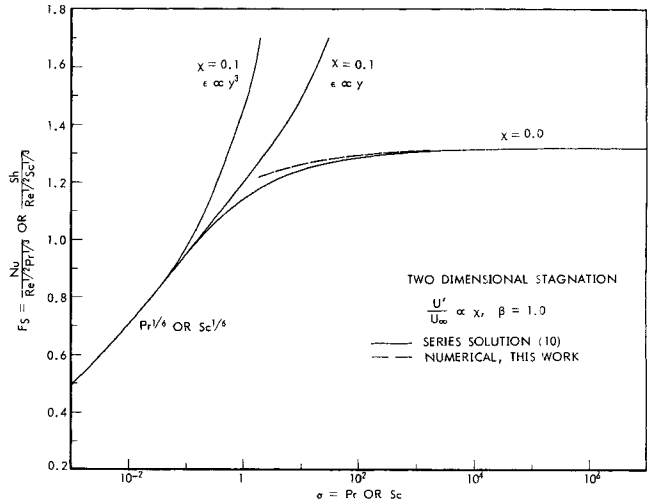

Fig. 9. Effect of boundary layer thickness.

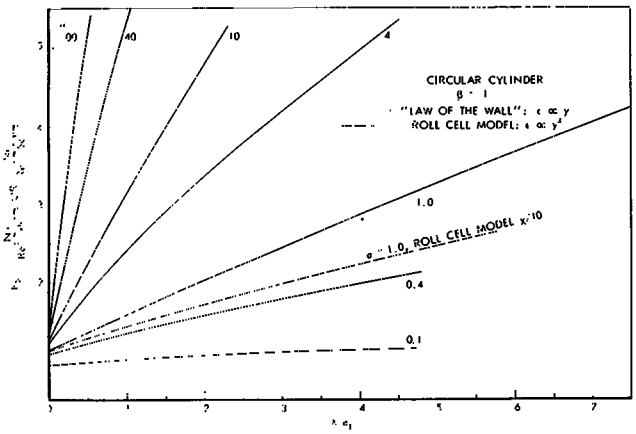

Fig. 10. Augmentation of Frossling number with turbulence.

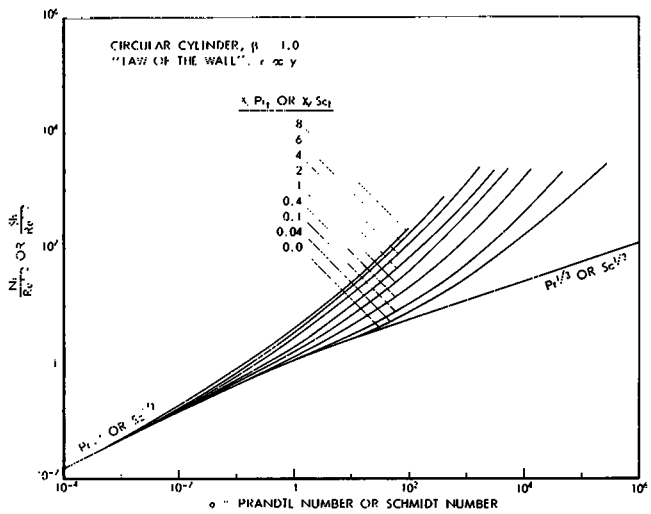

Fig. 11. Two-dimensional stagnation point, circular cylinder, $\beta = 1.0$.

pirically from Figure 8 as $B = 0.4328$ for $\beta = 1.0$. This represents an amazing agreement between theory and experiment.

The complete results of the first part of this theoretical study of the augmentation of forward stagnation point transport by boundary layer turbulence externally generated is presented using the simple law of the wall model for an example of two-dimensional flow ($\beta = 1.0$) in Figure 11 and axi-symmetric flow ($\beta = 0.5$) in Figure 12. It is obvious that the augmentation from effects of turbulence increases without bound as σ is increased and that for mass transfer involving liquids ($Sc \sim 10^3$) the augmentation can, indeed, be very large. The two cases $\beta = 1.0$ and 0.5 are simply related by a constant factor. The Frossling number for axi-symmetric geometry is just 1.1141 times larger than the result for two-dimensional geometry; therefore, in Equation (26) the coefficients A and B are simply related for the two cases. The general result becomes

$$F_s(1.1141)^{-k} = \frac{1.3215}{[1 + 0.5768(0.7554)^k \sigma^{-1/2}]^{1/3}} + 0.4328 \left(\frac{\chi}{\sigma_t}\right) \sigma^{1/6} \quad (27)$$

where $k = 0$ for two-dimensional symmetry and $k = 1$ for axi-symmetric flow.

The roll cell model expressed as $\epsilon \alpha y^3$ gave almost identical results as are shown in Figure 13 for two-dimensional flow ($\beta = 1.0$). For the same value of χ the augmentation of stagnation flow transport is larger; however, when the coefficient relating free-stream turbulence and χ is determined from experimental data the results are almost exactly identical as illustrated below.

For a specific system a critical comparison can be made between theory and experiment. Take the case of a circular cylinder placed transverse to a turbulently flowing air stream and the problem of predicting heat transfer from the cylinder to the air. For $\sigma \simeq \sigma_t \simeq 1$ Equation (26) reduces to

$$\frac{Nu}{Re^{1/2} Pr^{1/3}} = 1.1409 + 0.0426\, IRe^{1/2} \quad (28)$$

This equation has been shown in Figure 14 as the upper curve. Experimental data are shown for the effects of grid generated free stream turbulence on the forward stagnation point heat transfer from a 1.5 inch cylinder to air. (Galloway and Sage, 1967). The agreement is excellent for $\frac{u'}{U_\infty} Re^{1/2}$ below 15. Above 15 the data are significantly lower than the calculated curve, and this is believed to arise from the assumed constant σ_t and the simplified and

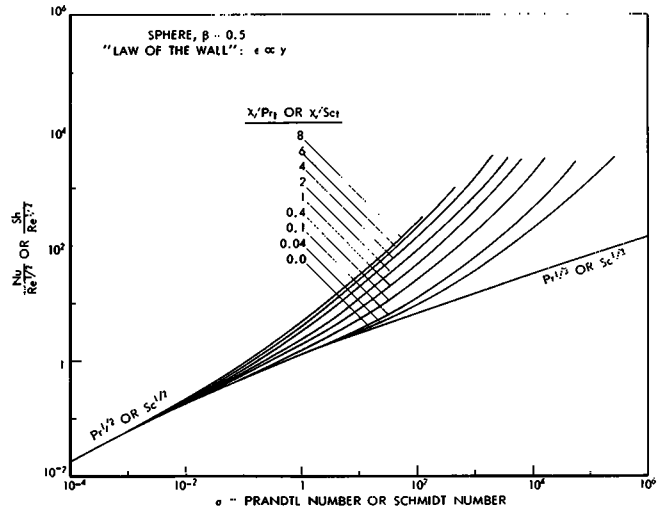

Fig. 12. Axi-symmetric stagnation point, sphere, $\beta = 0.5$.

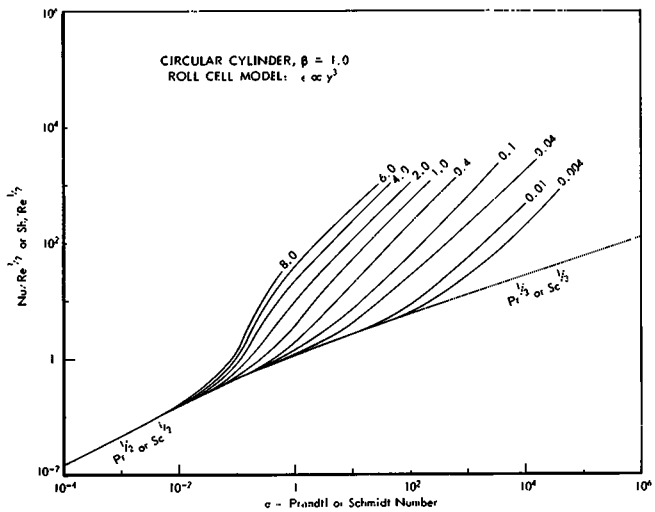

Fig. 13. Roll cell model augmentation at a two-dimensional stagnation point.

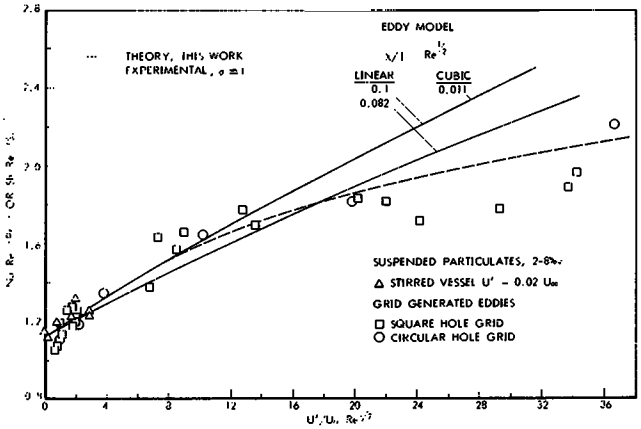

Fig. 14. Augmentation of forward stagnation point transport, comparison with experiments involving circular cylinders.

naive eddy law postulated in Equation (11) that idealizes as a wall effect the complex, unsteady three-dimensional roll cell structure near the surface, the complexity of which is fully illustrated in transition turbulent flow on flat plates (Runstadler et al. 1965) or near a forward stagnation point (Kuethe et al., 1961). Flow past bluff bodies is even further compounded by the fact that the potential flow field is not steady but fluctuates at the Strouhal shedding frequency and that this phenomenon greatly influences the transport process near separation (Galloway and Sage, 1967 and 1972). Effects near the forward stagnation are not large but undoubtedly are still present. Any refinement should bring in concepts of the unsteady, three-dimensional flow structure near the wall.

Figure 14 shows for comparison the curve for the law of the wall calculated by the present method using Smith's (1966) eddy proportionality of 0.164. It appears to predict slightly low just as for the skin friction in Figure 4. Therefore, in the present work, using the law of the wall, $\epsilon_m = 0.1\, IU_\infty y$ or $\chi = 0.1\, \frac{u'}{U_\infty} Re^{1/2}$ is preferred. This agrees well with the result $\epsilon_m = 0.097\, IU_x y$ established recently be Kearney et al., (1970) for effects of free stream turbulence on flat plate laminarization. For the roll cell model Figure 14 permits an evaluation of the dependence of the strength of roll cell circulation and their spacing. For a cubic model applied to the forward stagnation point of a cylinder, Equation (12) becomes

$$\chi_3 = \frac{\pi}{2u_1^{3/2}} \left(\frac{Ad}{U_\infty}\right) \left(\frac{d}{\lambda}\right) \tag{29}$$

corresponding to experimental conditions for Figure 14, $U_1 = 3.65$, and $\chi_3 = 0.011\, IRe^{1/2}$ there obtains

$$\chi_3 = 0.225 \left(\frac{Ad}{U_\infty}\right) \left(\frac{d}{\lambda}\right) = .011\, IRe^{1/2} \tag{30}$$

Using the results of Kestin and Wood (1970) for experimentally observed roll cell spacing

$$\frac{\lambda}{d} = \Lambda(I)\, \pi\, Re^{-1/2} \tag{31}$$

The circulation strength dimensionless group remains

$$\frac{Ad}{U_\infty} = 0.154\, I\, \Lambda\, (I) \simeq 0.193\, I \tag{32}$$

Since $\Lambda(I)$ depends only weakly on turbulence intensity this dimensionless circulation strength is nearly linearly related to turbulence intensity.

It is of interest to note that the physical mechanism of generating boundary layer turbulence does not matter. In essence one views a heat or mass transport enhancement possible when either an eddy in the free stream perturbs the stability of the laminar layer or a particle penetrates into this layer through impaction, thus upsetting the stability. For example, in Figure 14 are shown data for mass transfer to a sphere immersed in a suspension of fine particulates with a concentration around 5 volume %. The empirical expression $u' = 0.02\, U_\infty$ simply characterizes the equivalence between a slurry particle impacting into the laminar layer. The particle will impact rather than be swept past the surface when the particle Stokes number is above 1.32. The theory predicts that mass transfer augmentation will be observed for a particle Stokes number above its critical value for impaction, and this has been verified experimentally for the Stokes number ranging from 1.40 to 2.95. There are many other implications of such augmentation.

ACKNOWLEDGMENTS

The constructive comments and criticisms of S. F. Liang and D. A. Saville are greatly appreciated. L. E. Necoechea assisted in the digital computations. Appreciation is expressed to Dr. L. M. Blair, who performed the slurry enhancement experiments under the author's direction. And most of all, gratitude is expressed to the Shell Development Company for their permission to carry out much of this work and to release it for publication.

NOTATION

A = roll cell circulation strength, s^{-1}
A = coefficient of Equations (18), (22), (23), and (26)
b = coefficient of Equation (21)
B = coefficient of Equation (26)
C = time averaged concentration, kg/m^3
C_p = isobaric heat capacity, J/kg°K
c = instantaneous concentration, kg/m^3
c' = concentration fluctuation about C, kg/m^3
D = binary diffusion coefficient (from Chapman-Cowling), m^2/s
d = diameter of body, m
Fs = Frossling group defined by $(Nu \text{ or } Sh)/Re^{1/2}Sc^{1/3}$ for cylinders and $(Nu \text{ or } Sh - 2)/Re^{1/2}Sc^{1/2}$ for spheres
F = Merk function defined by Equation (1) such that $f_\eta\, (\xi, \eta) = U/U_1$
h = heat transfer coefficient, W/m^2°C
I = longitudinal turbulence of the free stream defined in Equation (4)
k = index describing flow symmetry as in Equation (1), $k = 0$ for two-dimensional flow and $k = 1$ for axi-symmetric flow
k = thermal conductivity, W/m²(°C/m)
K = mass transfer coefficient $= N/A\, (C_0 - C_\infty) =$ (m/s)
l = Prandtl's mixing length defined in Equation (2)
n = order of the Eddy law, defined in Equation (12)
N = mass flux, kg/s
Nu = time averaged Nusselt group $= hd/k$
Pr = Prandtl group $= \nu/\alpha$
P = total pressure − atmospheres (N/m^2)
Re = Reynolds group $= U_x d/\nu$
r, R = radial coordinate m
Sc = Schmidt group, ν/D

T = absolute temperature, °K
t = instantaneous absolute temperature, °K
T' = temperature fluctuations about T, °K
t = time s
U = time averaged velocity in the x direction, m/s
U_1 = velocity in the x direction immediately outside the boundary layer, m
u = instantaneous velocity in the x direction, m/s
u' = velocity fluctuations about U, m/s
V = time averaged velocity in the y direction, m/s
v = instantaneous velocity in the y direction, m/s
v' = velocity fluctuations about V, m/s
w = component velocity in the spanwise direction, m/s
x = component coordinate streamwise with the flow as defined in Figure 1, m
y = component coordinate normal to the surface as defined in Figure 1
z = component coordinate in the spanwise direction normal to both x and y, m

Greek Letters

α = thermal diffusivity, $k/\rho C_p$, m²/s
β = dimensionless pressure gradient or acceleration parameter defined in Equation (6)
ϵ = eddy coefficient, m²/s
ζ = dimensionless distance, $x/2R = x/d$
η = dimensionless similarity variable defined in Equation (1)
θ = dimensionless concentration $= (C - C_\infty)/(C_0 - C_\infty)$
λ = dimensionless roll cell wavelength function, defined in Equation (31)
Λ = roll cell wavelength spacing, defined in Equation (8) or (9), m
ν = kinematic viscosity, $(m^2/s) = \mu/\rho$
μ = viscosity of the media at position x, y, z, kg/m s
ξ = similarity variable defined in Equation (1)
ρ = density of the media at position x, y, z, kg/m²
σ = either Pr for heat transfer or Sc for mass transfer
ϕ_1 = functional relation defined in Equation (22) for cylinders
ϕ_2 = functional relation defined in Equation (23) for spheres
χ = turbulence parameter defined in Equation (5)
ψ = stream function defined by Equation (1)

Subscripts

A = molecular specie A
B = molecular specie B
d = of diffusion
h = of heat
m = of momentum
r = quantity defined for roll cell
t = quantity based on turbulent eddy coefficients (i.e., Equation 14)
0 = at the surface
1 = at a position immediately outside the boundary layer
∞ = in the free stream
η = denotes derivative with respect to η
ξ = denotes derivative with respect to ξ

LITERATURE CITED

Bird, R. B., W. E. Stewart, and E. H. Lightfoot, *Transport Phenomena*, Wiley, New York (1960).

Buyuktur, A. R., J. Kestin, and P. F. Meader, "Influence of Combined Pressure Gradient and Turbulence on the Transfer of Heat from a Plate," *Intern. J. Heat Mass Transfer*, 7, 1175 (1964).

Evans, H. L., *Laminar Boundary-Layer Theory*, Addison-Wesley, Mass. (1968).

Frossling, N., "Evaporation, Heat Transfer, and Velocity Distribution in Two-Dimensional Potentially Symmetric Laminar Boundary Layer Flow," NACA TM-1432 (1958).

Galloway, T. R., "A Study on the Mechanism of Molecular Transport with Systems of Gaseous Paraffins and of Convective Transport from Single Cylinders, Single Spheres, and Arrays of Spheres into Turbulently Flowing Streams," Ph.D. dissertation, Calif. Instit. Technology, Univ. Microfilm Report No. 67-10 (1967).

———., and B. H. Sage, "Thermal and Material Transfer in Turbulent Gas Streams—A Method of Prediction for Spheres," *Intern. J. Heat Mass Transfer*, 7, 783 (1964); 10, 413 (1967).

———., "Local and Macroscopic Transport from a 1.5-Inch Cylinder in a Turbulent Air Stream," *AIChE. J.*, 13, 563 (1967).

———., "Local and Macroscopic Thermal Transport From a Sphere in a Turbulent Air Stream," *ibid.*, 18, 287 (1972).

Gortler, H., "A New Series for the Calculation of Steady Laminar Boundary Layer Flows," *J. Math. Mechanics*, 6, 1 (1957); with detailed numerical results available at Harvard Univ. Comput. Lab., problem report No. 85, by Mr. Gerard Salton, August 1954.

Junkhan, G. H., and G. K. Serovy, "Effects of Free-Stream Turbulence and Pressure Gradient on Flat-Plate Boundary-Layer Velocity Profiles and on Heat Transfer," *Trans. ASME, J. Heat Transfer*, 89, 169 (1967).

Kearney, D. W., et al. "The Effect of Free-Stream Turbulence on Heat Transfer to a Strongly Accelerated Turbulent Boundary Layer," *Proc. 1970 Heat Transfer Fluid Mechanics Inst.* (1970).

Kestin, J., P. F. Maeder, and W. E. Wang, "Influence of Turbulence on the Transfer of Heat from Plates with and Without a Pressure Gradient," *Intern. J. Heat Mass Transfer*, 3, 133 (1961).

Kestin, J., and R. T. Wood, "On Stability of Two-Dimensional Stagnation Flow," *J. Fluid Mechanics*, 44, 461 (1970).

Kuethe, A. M., W. W. Willmarth, and G. H. Crocker, "Turbulence Field Near the Stagnation Point on Blunt Bodies of Revolution," in *Proc. Heat Transfer Fluid Mechanics Inst.*, pp. 10-22, Stanford Univ. Press, Calif. (1961).

Merk, H. J., "Rapid Calculations for Boundary-Layer Transfer Using Wedge Solutions and Asymptotic Expansions," *J. Fluid Mechanics*, 5, 460 (1959).

Rosenhead, L. (Ed.), *Laminar Boundary Layers*, Oxford Univ. Press, London (1963).

Ruckenstein, E., and C. Berbente, "The Effect of Roll Cells on Mass Transfer," *Chem. Eng. Sci.*, 25, 475 (1970).

Runstadler, P. W., S. J. Kline, and W. C. Reynolds, "An Investigation of the Flow Structure of the Turbulent Boundary Layer," Report MD-8 Thermosciences Div., Mech. Eng. Dept., Stanford Univ. (1965).

Sadeh, W. Z., S. P. Sutera, and P. F. Meader, "Analysis of Vorticity Amplification in the Flow Approaching a Two-Dimensional Stagnation Point," *ZAMP 21*, Fasc. 5, 699 (1970) and "An Investigation of Vorticity Amplification in Stagnation Flow," *ibid.*, p. 717.

Schlichting, H., *Boundary Layer Theory*, McGraw-Hill, New York (1960).

Smith, M. C., and A. M. Kuethe, "Effects of Turbulence on Laminar Skin Friction and Heat Transfer," *Phys. Fluids*, 9, 2337 (1966).

Squire, U. B., "Heat Transfer Calculations for Aerofoils," ARC Reports and Memoranda, No. 1986 (1942).

Sutera, S. P., "Vorticity Amplification in Stagnation-Point Flow and Its Effect on Heat Transfer," *J. Fluid Mechanics*, 21, 513 (1965).

———., P. F. Maeder, and J. Kestin, "On the Sensitivity of Heat Transfer in the Stagnation-Point Boundary Layer to Free-Stream Vorticity," *ibid.*, 16, 497 (1963).

Coles, D. E., and E. A. Hirst, (Eds.), Thermosciences Div., "Computation of Turbulent Boundary Layers—1968, AFOSR-IFP-Stanford Conf," *Proc.*, Vol. I and II, Stanford Univ., Calif. (1968).

Manuscript received November 10, 1972; revision received December 29, 1972, and accepted January 2, 1973.